Cite this: DOI: 10.1039/c0xx00000x

www.rsc.org/xxxxxx

ARTICLE TYPE

Fullerene-driven encapsulation of a luminescent Eu(III) complex in carbon nanotubes

Laura Maggini,[a,b] Melinda-Emese Füstös,[c,d] Thomas W. Chamberlain,[e] Cristina Cebrián,[b] Mirco Natali,[b,f] Marek Pietraszkiewicz,[g] Oksana Pietraszkiewicz,[g] Edit Székely,[h] Katalin Kamarás,[c] Luisa De Cola,[b] Andrei N. Khlobystov[e] and Davide Bonifazi*[a,i]

Received (in XXX, XXX) Xth XXXXXXXXX 20XX, Accepted Xth XXXXXXXXX 20XX
DOI: 10.1039/b000000x

A novel CNT-based hybrid luminescent material was obtained *via* encapsulation of a C_{60}-based Eu(III) complex into single-, double- and multi-walled carbon nanotubes (SWCNTs, DWCNTs and MWCNTs, respectively). Specifically, a luminescent negatively-charged Eu(III) complex, electrostatically bonded to an imidazolium-functionalized fullerene cage, was transported inside CNTs by exploiting the affinity of fullerenes for the inner surface of these carbonaceous containers. The filling was performed under supercritical CO_2 ($scCO_2$) conditions to facilitate the entrapment of the ion-paired assembly. Accurate elemental, spectroscopic and morphological characterization not only demonstrated the efficiency of the filling strategy, but even the occurrence of a nano-ordering of the encapsulated supramolecular luminophores when SWCNTs were employed. Preliminary confocal microscope imaging studies showed that these hybrids could have some potential for diagnostic applications.

Introduction

Along with an increase of the available methodologies for their manipulation,[1] and the development of atomic-resolution visualization techniques, mainly high-resolution transmission electron microscopy (HRTEM),[2] current efforts in carbon nanotube (CNT)[3] research are directed towards the study and exploitation of their porous properties. Indeed, CNTs can be employed as nano-containers, nano-reactors, or as fillable conductive nano-vessels, able to give rise to advanced hybrid graphitic materials utilizable in electronic devices.[4]

The feasibility of the entrance of guest molecules within the inner channel of CNTs relies on the favorable establishment of a range of interactions between the "guest" molecules and the "host" CNTs,[5] amongst which van der Waals forces often appear to be predominant.[6] These are maximized when the host–guest complex occurs between CNTs and related graphitic materials,[7] such as fullerenes, *e.g.* C_{60} and C_{70}. In fact, the common nature of the two materials, together with the perfect geometrical match of the shape of a fullerene and the inner nanotube surface of single-walled CNTs (SWCNTs), results in a spontaneous encapsulation.[8]

The use of CNTs as templating nano-containers has recently started to draw attention as a possible strategy for the synthesis of novel highly organized photonic materials. It is well established that the emission properties of a chromophore, in terms of color and intensity, are extremely sensitive to the environment.[9] Encapsulation of luminophores within a protective "cage" (*i.e.* CNTs) might hence grant a sheltering effect from hostile reactive species, as *Yanagi et al*. demonstrated with the encapsulation of *β*-carotene within SWCNTs,[12] allowing longer-lasting luminescence performances of the hosted molecules. Furthermore, molecular confinement in such a restrained space might induce a well-ordered mono-dimensional molecular arrangement, potentially characterized by unique emission

[a] *Dr. L. Maggini, Prof. Dr. D. Bonifazi, Namur Research College (NARC), University of Namur (UNamur). Rue de Bruxelles 61, 5000 Namur Belgium E-mail: davide.bonifazi@unamur.be*
[b] *Dr. L. Maggini, Dr. C. Cebrián, M. Natali, Prof. Dr. L. De Cola, Institut de Science et d'Ingénierie Supramoléculaires (ISIS), Alleé Gaspard Monge 8, 67000 Strasbourg, France*
[c] *M.E. Füstös, Prof. Dr. K. Kamarás, Institute for Solid State Physics and Optics, Wigner Research Centre for Physics, Hungarian Academy of Sciences. Konkoly-Thege M. 29-33, 1121 Budapest, Hungary*
[d] *M.E. Füstös, Faculty of Chemistry and Chemical Engineering, Babeş -Bolyai University, Arany János 11, 400028 Cluj-Napoca, Romania*
[e] *Dr. T. W. Chamberlain, Prof. Dr. A. N. Khlobystov, School of Chemistry, University of Nottingham, University Park, Nottingham NG7 2RD, UK*
[f] *M. Natali, Department of Chemical and Pharmaceutical Sciences, University of Ferrara, Via Fossato di Mortara 17-19, 44121, Ferrara, Italy*
[g] *Prof. Dr. M. Pietraszkiewicz, Dr. Oksana Pietraszkiewicz, Institute of Physical Chemistry, Polish Academy of Sciences, PL-01224 Warsaw, Kasprzaka 44/52, Poland*
[h] *Dr. Edit Székely, Department of Chemical and Environmental Process Engineering, Budapest University of Technology and Economics, Budafoki út 8, 1111 Budapest, Hungary*
[i] *Prof. D. Bonifazi, Department of Chemistry and Pharmaceutical Sciences, INSTM UdR Trieste, University of Trieste (UNITS), Piazzale Europa 1, 34127 Trieste Italy*

† Electronic Supplementary Information (ESI) available: [Experimental details, XPS, TGA, ATR-IR and PL analysis, additional HRTEM and confocal images]. See DOI: 10.1039/b000000x/

properties. At present only a relatively limited number of luminescent guests have been successfully inserted inside CNTs and their light emitting properties investigated.[13] Among these, a prime example of the templating action of CNTs on internalized luminescent molecules has been described for the encapsulation of coronenes in SWCNTs.[14-15]

Lanthanide β-diketonate complexes (LnCs)[16] are among the most investigated rare earth coordination compounds. Regrettably, despite their exceptional luminescent properties, their low thermal and photochemical stability,[17] together with their tendency to aggregate undergoing quenching inter-chromophoric interactions, often limit their utilization in electro-luminescent devices. Taking advantage of several scaffolding materials, attempts to enhance the mechanical properties of LnCs have been accomplished.[16,18-19] In a collaborative effort, we first reported a simple and straightforward methodology to prepare LnC-CNTs hybrids by direct adsorption of a neutral Eu(III)-based LnC onto oxidized single-walled CNTs (ox-SWCNTs) *via* hydrophobic interactions, obtaining a strongly emitting composite in which the structural and electronic properties of both constituents remained preserved.[20] Since then, different approaches to blend CNTs and LnCs have been reported.[21-24] Among these, our group specifically developed new exohedral supramolecular functionalization methodologies with Eu(III)-based complexes.[25-27] In particular, by means of electrostatic interactions, negatively charged Eu(III) complexes were used to positively decorate charged multi-walled CNTs (MWCNTs) forming stable and luminescent hierarchized architectures.

Intrigued by the possibility of exploring the effect of encapsulation on the luminescent output of LnCs, we have recently tackled the filling of MWCNTs with a neutral and hydrophobic *tris*-hexafluoro acetylacetonate Eu(III) complex, using the nano-extraction methodology.[28] Dismally, the as-prepared hybrid resulted in poor loading and consequently displayed weak emission properties. Hence, with the aim to improve both the filling load and the luminescence of the resulting hybrid material, we decided to exploit the unique CNT-C_{60} interaction to vehiculate LnCs inside CNTs. Inspired by the "nano-carriers" approach as developed by *Khlobystov et al*.[29] who demonstrated the effectiveness of using fullerenes as vehicles for inserting transition metal complexes inside SWCNTs, we also decided to use C_{60} to facilitate and direct the entrance of the LnC within the carbonaceous cavity.

To pursue our goal, we selected the bright *tetrakis*(2-naphtoyltrifluoro-acetonato) Eu(III) complex ($[\mathbf{EuL_4}]\cdot\mathbf{NEt_4}$)[18a,30] as a guest molecule. This negatively charged compound is known from literature to efficiently interact with imidazolium-based ionic liquids (ILs)[25,31-32] through both electrostatic and cation-π interactions. Hence, we performed the synthesis of a C_{60} derivative bearing an imidazolium appendage (**1**·**Br**) capable of ion-pairing with $\mathbf{[EuL_4]^-}$. The resulting ion-paired complex (**1**·[$\mathbf{EuL_4}$], Scheme 1) is thus composed of a luminescent "tail", and a fullerene "head", with the latter in charge of directing and assisting the encapsulation of the LnC within the inner channel of CNTs. Such design should not only ensure easier encapsulation of the luminescent module within the CNTs, but, more interestingly, it should also control the nano-structuration within the channel of CNTs with the fullerene moieties of each encapsulated assembly pointing in the same direction, insulating the LnCs. The C_{60}-based assembly was then employed in a supercritical CO_2 ($scCO_2$) induced encapsulation procedure inside single-, double- and multi-walled CNTs (SWCNTs, DWCNTs and MWCNTs) in order to test the difference in encapsulation efficiency as a result of changing the nanotube structure (number of graphitic layers, diameter of the inner channel, to name a few). Comprehensive characterization was carried out with X-ray photoelectron spectroscopy (XPS) and thermogravimetric analysis (TGA) to determine the elemental and quantitative composition of the hybrids and high-resolution transmission electron microscopy (HRTEM) to unravel the structural morphology. Attenuated total reflectance infrared (ATR-IR) and photoluminescence studies (PL) were used to study the spectroscopic properties of the encapsulated hybrids. Preliminary i*n-vitro* cellular uptake studies using a confocal microscope have also been performed.

Results and discussion

Synthesis

The C_{60}-based positively charged nano-carrier (**1**·**Br**) was synthesized as shown in Scheme 1. Initially, C_{60} was subjected to a 1,3-dipolar cycloaddition reaction in the presence of the azido-functionalized imidazolium-based ionic liquid **5**. The latter was synthesized starting from ethyl-imidazolium, which was first alkylated with 5-bromo-pentanol, affording the oxydrilated derivative **3**. Subsequent bromination *via* Appel reaction in the presence of CBr_4 and PPh_3 (**4**), followed by nucleophilic substitution of the terminal Br with the azido functional group provided desired ionic liquid **5** (Scheme 1). Anion exchange metathesis reaction yielding supramolecular complex **1**·[$\mathbf{EuL_4}$] was performed by simply stirring a dispersion of the C_{60}-appended ionic liquid carrier (**1**·**Br**) with an excess of precursor ionic complex $[\mathbf{EuL_4}]\cdot\mathbf{NEt_4}$ (10 equivalents) in toluene for 14 hours in the air and at r.t.

Due to their low viscosity, absence of surface tension, and low solvation effect, supercritical fluids (SCFs) provide high diffusivity, approaching that of the gas phase.[33] Among these, supercritical CO_2 ($scCO_2$) revealed to be particularly efficient for preparing peapods,[34-35] and for this reason we have decided to use $scCO_2$ as a solvent in the preparation of this luminescent hybrid.[36] Prior to the encapsulation reaction, CNTs were oxidized[37] to remove their endcaps. Subsequently, the carbonaceous species were annealed in air at 570 °C for 20 minutes to remove any carboxylic groups that could hamper the efficient insertion of the nano-carrier. Encapsulation was finally performed at 50 °C and 150 bar for 96 hours, followed by extensive washing by CH_2Cl_2 to remove any **1**·[$\mathbf{EuL_4}$] physisorbed on the external wall of the CNTs (Fig. S1, S.I.).

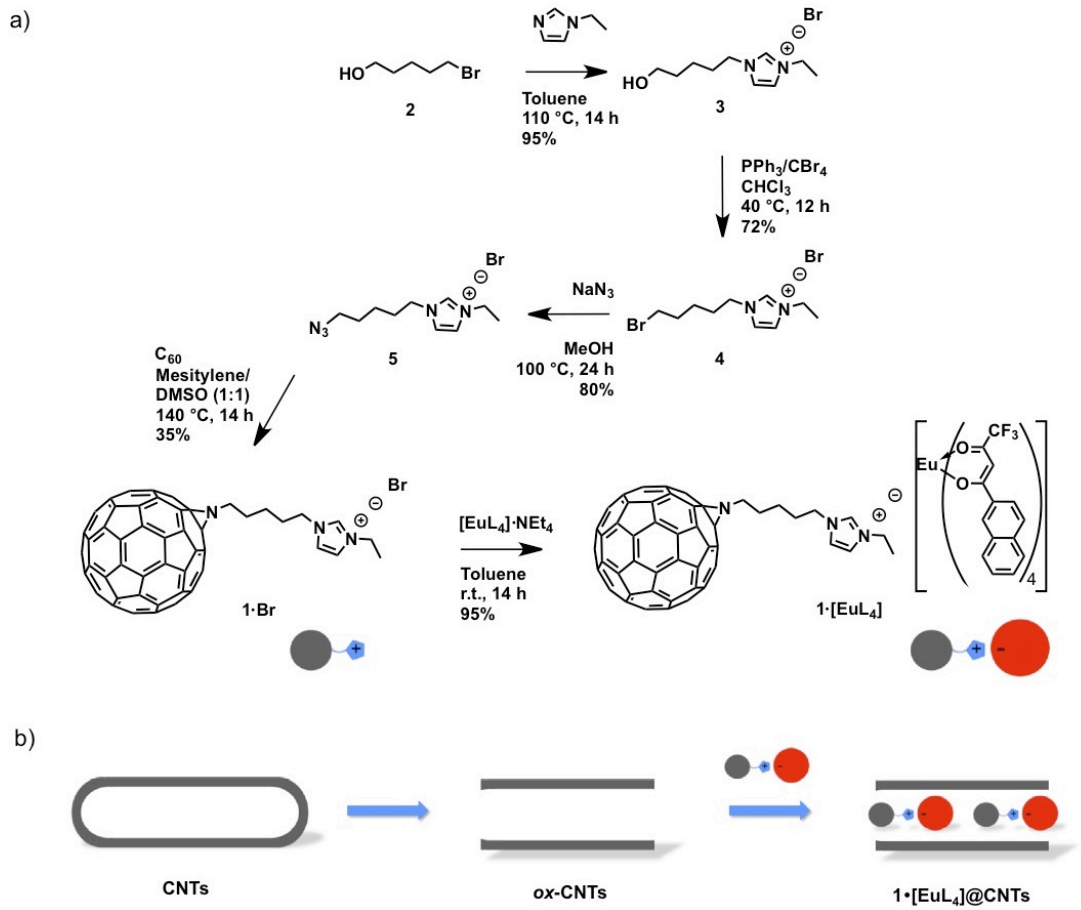

Scheme 1. a) Synthetic procedures for preparing supramolecular complex **1·[EuL$_4$]**. b) Schematic representation of the filling approach for encapsulating ion-paired complexes..

Qualitative and quantitative characterization of the hybrid material

The elemental composition of the synthesized modified peapods was firstly assessed by XPS analysis. As shown in Table 1 (see also Fig. S2-3, S.I.), the oxidized CNTs (**ox-SWCNTs**, **ox-DWCNTs** and **ox-MWCNTs**) only presented the C (1s) and the O (1s) signals at 284 and 533 eV, respectively. The signals relative to **1·[EuL$_4$]**, namely Eu (3d) (1134 eV), F (1s) (686 eV) and N (1s) (401 eV) were detected for **1·[EuL$_4$]@SWCNTs** and **1·[EuL$_4$]@DWCNTs**, whereas hybrid **1·[EuL$_4$]@MWCNTs** exhibited only the signals of N (1s) and F (1s) alongside peculiar signals from the CNTs. The absence of the signal of Eu (3d) is due, not only to a lower amount of encapsulated LnC, but also to the decrease in sensitivity of this analytical technique in the detection of the encapsulated material when increasing the number of graphitic layers of the CNTs (*vide infra*).

TGA analysis of **1·[EuL$_4$]@CNTs** (Fig. 1; see also Fig. S4-5, S.I.) confirmed the trend observed *via* XPS analysis. Specifically, in the case of **1·[EuL$_4$]@SWCNTs** and **1·[EuL$_4$]@DWCNTs** the TGA plot revealed two thermal decomposition events. The first event, starting at around 400 °C, is assigned as decomposition of the encapsulated LnC. The second event, beginning at 550 °C, is the result of the decomposition of the carbon materials: namely the CNT framework and the encapsulated C_{60}. This assignment is in agreement with previously reported TGA observations for encapsulated Eu(III) complex and fullerene peapods, for which the entrapped material resulted characterized by a higher combustion temperature, as compared to the free species because of the shielding effect of the CNTs sidewalls.[25,38] Before discussing the extent of the weight

Table 1. XPS atomic percentage values obtained for ox-CNTs, and the related encapsulated derivatives.[a]

	C[%][b]	O[%][b]	N[%][b]	F[%][b]	Eu[%][b]
ox-SWCNTs	96.8 ± 0.6	3.2 ± 0.6	-	-	-
1·[EuL$_4$]@SWCNTs	89.0 ± 0.8	4.4 ± 0.3	0.3 ± 0.1	6.2 ± 0.6	0.1 ± 0.05
ox-DWCNTs	95.6 ± 0.1	4.4 ± 0.1	-	-	-
1·[EuL$_4$]@ DWCNTs	91.2 ± 0.2	5.2 ± 0.3	1.3 ± 1.0	2.2 ± 0.4	0.1 ± 0.05
ox-MWCNTs	97.4 ± 0.9	2.6 ± 0.9			
1·[EuL$_4$]@ MWCNTs	96.5 ± 0.4	2.0 ± 0.2	1.3 ± 0.2	1.3 ± 0.2	-

[a]Each value is the average of three measurements of the sample. [b]Atomic percentage.

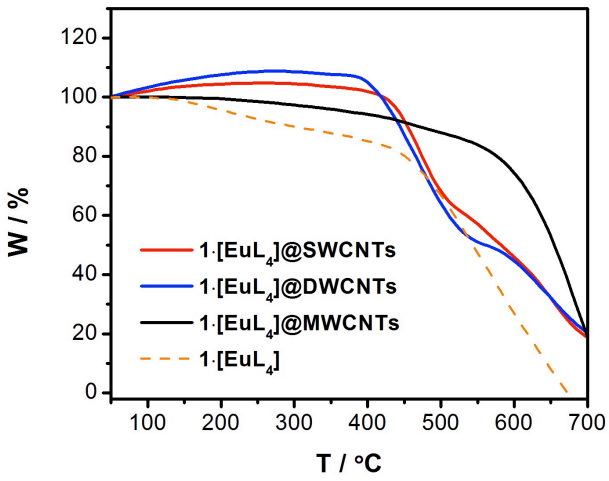

Figure 1. TGA traces for **1**·[**EuL**$_4$]**@SWCNTs** (red line), **1**·[**EuL**$_4$]**@DWCNTs** (blue line) and **1**·[**EuL**$_4$]**@MWCNTs** (black line). The supramolecular nano-carrier **1**·[**EuL**$_4$] is also reported for comparison (orange dashed trace). The analysis was recorded in N_2/air (80:20) atmosphere with a heating ramp of 2° C / min.

Table 2. TGA analysis data of the **1**·[**EuL**$_4$]**@CNTs** hybrids.[a]

	TGA [% loss]	[μmol/mg][b]
1·[**EuL**$_4$]**@SWCNTs**	36.6	0.4
1·[**EuL**$_4$]**@DWCNTs**	47.8	0.5
1·[**EuL**$_4$]**@MWCNTs**	10.4	0.1

[a]All the experiments were carried out in N_2/air (80:20) atmosphere with a temperature ramp of 2 °C/min. [b]Calculated considering that all the organic material decomposed was part of complete [**EuL**$_4$]$^-$ moieties.

loss, it has to be pointed out that both the TGA traces of **1**·[**EuL**$_4$]**@SWCNTs** and **1**·[**EuL**$_4$]**@DWCNTs** present a slight weight increase before 400 °C, temperature at which the decomposition of captured **1**·[**EuL**$_4$] begins (see Fig. S5). This phenomenon is most probably due to the presence of residual catalyst particles in the CNT samples undergoing oxidation when heated in air (Fig. S5).[39] Contribution to this phenomenon in the case of DWCNTs might also derive from some Eu(III) complex which, entering the CNTs, might have undergone a transformation into metallic Eu particles (Fig. 2c), species prone to oxidation. However, the extent of the weight loss centered at 450 °C regards exclusively the organic part of the luminescent [**EuL**$_4$]$^-$. Considering this, it was hence possible to assess the amount of LnC encapsulated, 0.4 and 0.5 μmol/mg for SWCNTs and DWCNTs hybrids respectively (see Table 2). **1**·[**EuL**$_4$]**@MWCNTs** only presented a trivial, yet detectable, weight loss episode.

Morphological characterization

The structure of the resultant endohedral hybrid material was investigated *via* high-resolution transmission electron microscopy (HRTEM). During the analysis, the energy of the electron beam (e-beam) was lowered to avoid knock-on damage caused by the collision of electrons from the e-beam with the atoms of the sample. However, decomposition of **1**·[**EuL**$_4$] was observed even at 100 kV, often causing just partial visualization of the complex. However, significant amounts of material were observed within

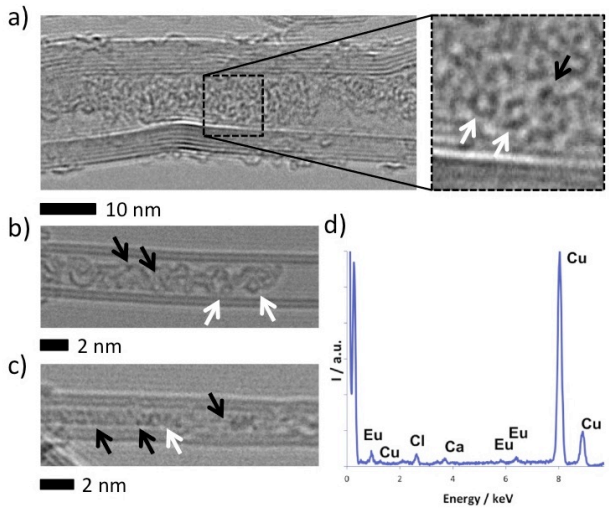

Figure 2. HRTEM images taken at 100 kV of a) **1**·[**EuL**$_4$]**@MWCNTs** showing large amounts of material within the nanotube channel, the enlarged region shows both fullerene cages (white arrows) and Eu metal atoms (black arrow) which is indicative of successful encapsulation of the Eu complex. b-c) **1**·[**EuL**$_4$]**@DWCNTs** where fullerene cages and significant amounts of Eu metal are observed, the elongated metal cluster present in c) is a result of e-beam decomposition of the Eu complex followed by aggregation of the metal atoms to form a rod like structure templated by the shape of the nanotube cavity. d) The energy dispersive X-ray (EDX) spectrum of the **1**·[**EuL**$_4$]**@DWCNTs** confirms the presence of Eu within the nanotubes (Cu peaks are due to the TEM specimen grid and Cl is from the solvent used for sample preparation.)

the internal channel of both MWCNTs and DWCNTs (Fig. 2; see also Fig S6-7, S.I.). Specifically, fullerene cages were clearly spotted throughout both samples: in the case of DWCNTs the **1**·[**EuL**$_4$] units appear well separated, whereas inside MWCNTs the nano-carriers appear tightly agglomerated and clustered. The consistant presence of Eu(III) ions within the DWCNTs, highlighted by the detection of dark spots in the HRTEM images, was also confirmed *via* energy dispersive X-ray (EDX) spectroscopy. Nevertheless, in this sample some Eu metal clusters were also detected, probably formed by complex decomposition followed by free metal atoms agglomeration (Fig. 2c).

More interestingly, **1**·[**EuL**$_4$]**@SWCNTs** exhibited distinct organization. Indeed, several fullerene cages were observed within the internal cavity of SWCNTs characterized by an internal diameter equal or higher than 2.7 nm (Fig. 3), which corresponds to the minimum diameter required for containing **1**·[**EuL**$_4$] (Fig. 3e). In smaller tubes, mainly naked C_{60} units were detected. This phenomenon can be explained by taking into account the diameter and the lack of flexibility of the Eu(III) complex. Indeed, **1**·[**EuL**$_4$] shows a critical diameter of 2.4 nm and is too large to fit within standard SWCNTs (diameter typically around 1.4 nm). In this case, the complex is not able to adjust its conformation in order to squeeze in these tubes, and as it is predicted that the energy gained from the fullerene part of the complex entering the nanotube is significantly larger than the electrostatic interaction holding the "nano-carrier" together, the supramolecular complex will dissociate, with the Eu component stripped off from the fullerene cage (Fig. S8, S.I.). Similar phenomena were previously reported for fullerene metal complexes which are too large to fit within SWCNTs.[40] Nevertheless, several **1**·[**EuL**$_4$] were found in wider than average

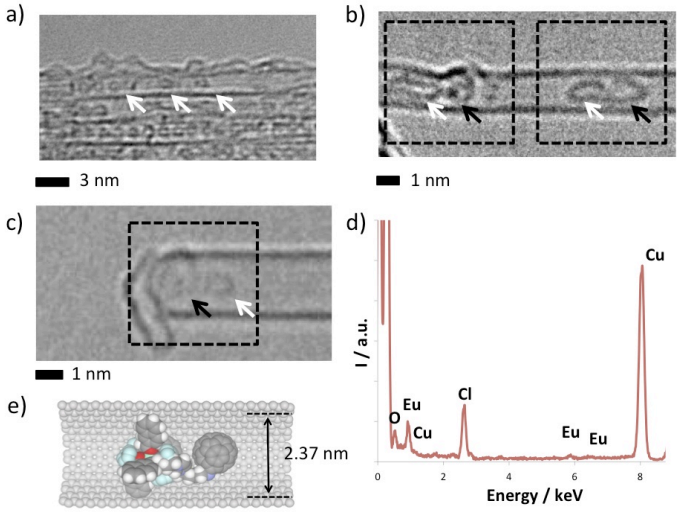

Figure 3. HRTEM images taken at 100 kV of a-c) the material obtained from attempts to encapsulate the **1**·[**EuL$_4$**] in SWCNTs. a) Significant numbers of fullerene cages (white arrows) are observed within standard SWCNTs' channels. b-c) In wider SWCNTs (d_{NT} = 2.8 nm), the complex is intact and is clearly discernable the presence of the fullerene cage (white arrow) and that of the Eu atom (black arrow). d) EDX spectrum of **1**·[**EuL$_4$**]**@SWCNTs**. e) Schematic representation of the complex **1**·[**EuL$_4$**] within a wide SWCNTs.

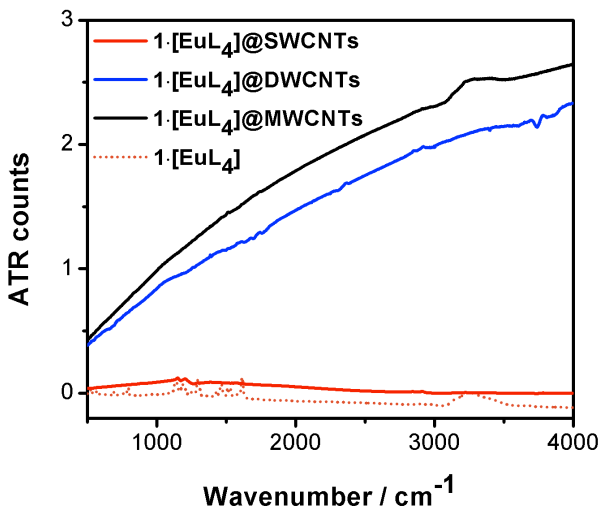

Figure 4. ATR-IR spectra for **1**·[**EuL$_4$**] and the nanotube hybrids. No vibrational peaks are discernible in the hybrids, indicating that exohedrally adsorbed species have been completely removed by washing.

SWCNT (d_{CNT} = 2.7 nm) present in the sample, as clearly evidenced in Figures 3b-c. The supramolecular nano-carrier **1**·[**EuL$_4$**] appears as a fullerene cage (white arrow) followed by a dark spot in close proximity, assigned to the single Eu atom. The organic ligands of the Eu(III) complex, being incredibly susceptible to e-beam damage due to the high number of hydrogen atoms present (immediately stripped out by the e-beam at 100 kV), appear as an area of grey contrast around the Eu atom. Even though intact **1**·[**EuL$_4$**] were unable to enter standard SWCNTs, the amount present in the larger than average tubes behaved as expected. Indeed, when several **1**·[**EuL$_4$**] assemblies were observed along the same tube, it was evidenced that the orientation of the single assembly was coherent with that of the others, proving the efficient role of the C_{60} as directing agent in the encapsulation procedure. Moreover, a certain degree of regularity in the spacing between the units could be observed, indicating isolation of the luminophores within the structure by C_{60} cages of neighbouring molecules thus preserving their luminescent properties by preventing parasite inter-chromophoric quenching phenomena.

Spectroscopic characterization of the hybrid

While electron microscopy reveals the encapsulated species, it is still important to exclude the presence of adsorbed **1**·[**EuL$_4$**] on the nanotube surfaces in order to unambiguously assign the spectroscopic features of the encapsulated molecules. Attenuated total reflectance infrared (ATR-IR) spectroscopy was therefore performed to exclude the presence of exohedrally adsorbed material in the hybrid structures (Fig.4; see also Fig. S9, S.I.).

In fact, it has been previously shown[36] that ATR spectroscopy on CNT hybrids does not detect encapsulated species, but only adsorbed ones. Thus the lack of the ATR signals of **1**·[**EuL$_4$**], demonstrates the absence of adsorbed assemblies on the external surface in the purified hybrids. We conclude that the majority of the Eu(III) derivative present in the sample is inside the nanotubes.

Photophysical characterization (PL) of the encapsulated hybrids, **1**·[**EuL$_4$**]**@CNTs**, was hence accomplished in the solid state. As displayed in Figure 5, upon exciting the investigated **1**·[**EuL$_4$**]**@CNTs** samples at 375 nm (see Fg. S10, S.I.), the typical emission spectrum of the Eu(III) ion, characterized by several emission features between λ = 570 and 700 nm,[36] was detected. Specifically, the fingerprint emission of Eu(III) arises from $^5D_0 \rightarrow {}^7F_J$ (J = 0–4) electronic transitions. Among others, electric ($^5D_0 \rightarrow {}^7F_2$) and magnetic ($^5D_0 \rightarrow {}^7F_1$) dipolar transitions are predominant in the regions λ = 610 to 625 and 585 to 600 nm, respectively.

The position of the maximum of the "hypersensitive" electric dipolar transition $^5D_0 \rightarrow {}^7F_2$,[41] slightly blue shifts from λ = 614 nm of **1**·[**EuL$_4$**] to 613 and 612 nm for **1**·[**EuL$_4$**]**@SWCNTs** and **1**·[**EuL$_4$**]**@DWCNTs**, and then red-shifts to 615 nm for **1**·[**EuL$_4$**]**@MWCNTs**. At the contrary, the magnetic dipole transition $^5D_0 \rightarrow {}^7F_1$, largely independent of the ligand field,[42] remained practically unvaried ($\lambda \approx$ 591 nm). The intensity ratio between the electric dipole transition and the magnetic dipole transition (R_{21}) affords straightforward indication of the change in the coordination symmetry of a LnC.[43] A value of 36 resulted for both **1**·[**EuL$_4$**] and **1**·[**EuL$_4$**]**@SWCNTs**, whilst it decreased to 34 for **1**·[**EuL$_4$**]**@DWCNTs** and then to 8 for **1**·[**EuL$_4$**]**@MWCNTs**, suggesting that [**EuL$_4$**]$^-$ only preserves the symmetry of its free form inside the larger SWCNTs. The absence of distortions support the occurrance of an ordered encapsulation in which the Eu(III) complexes are mainly isolated and organized within the CNT channel, confirming the HRTEM results. For DWCNTs and MWCNTs, the higher disorder evidenced by HRTEM images reflects a higher distortion of the Eu(III) complex.

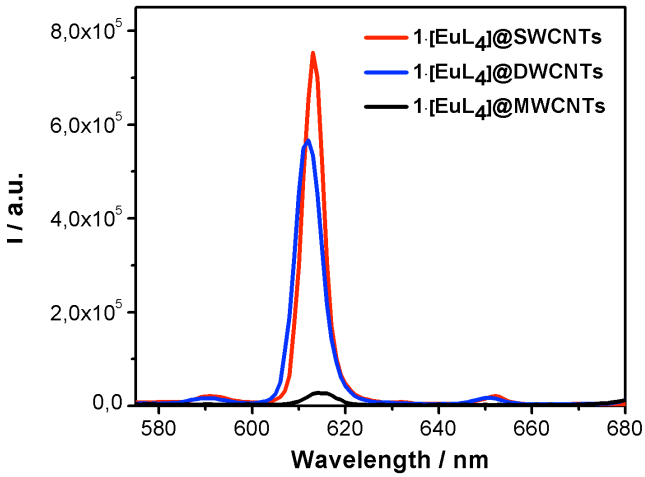

Figure 5. Emission profiles (λ_{exc} = 375 nm) of KBr pellets (1 mg of encapsulated material mixed with 10 mg of KBr) containing **1·[EuL$_4$]@SWCNTs** (red trace), **1·[EuL$_4$]@DWCNTs** (blue trace), and **1·[EuL$_4$]@MWCNTs** (black trace). .

Table 3. Photophysical data for **1·[EuL$_4$]@CNTs** hybrids.

	λ_{em}[a] [nm]	τ[b] [μs]	PLQY(%)[c]
1·[EuL$_4$]	614	256	13
1·[EuL$_4$]@SWCNTs	613	2.40 (20%), 0.17 (80%)	0.02
1·[EuL$_4$]@DWCNTs	612	1.49 (40%), 0.25 (60%)	0.03
1·[EuL$_4$]@MWCNTs	615	0.18 (40%), 0.08 (60%)	0.004[d]

[a]at room temperature, λ_{exc} = 375 nm; [b] at room temperature, λ_{exc} = 375 nm, analyzed at 614 nm; [c]calculated quantum yields according to Eq 1,2; [d]estimated quantum yields assuming the same τ_{rad} value as for SWCNTs and DWCNTs.

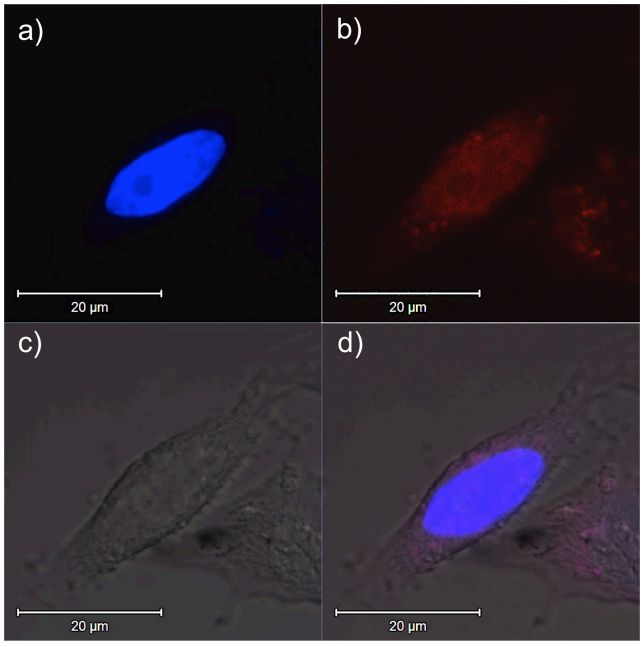

Figure 6. Confocal microscope images of HeLa cells incubated for 24 h with **1·[EuL$_4$]@SWCNTs**, wrapped in PEG-5000 polymer. a-c) Separation of the different detected signals: a) DAPI channel (excitation wavelength = 405 nm, detection wavelength between 400 and 600 nm); b) Eu(III) channel (excitation wavelength = 405 nm, detection wavelength = 614 nm); c) PMT channel; d) overlap of the channels.

The effect of the different packing motifs is further observable following the emission quantum yields and lifetimes. In fact, along the series from SWCNTs to MWCNTs, the hybrids result characterized by increasingly lower emission quantum yields and shorter excited state lifetimes compared to reference **1·[EuL$_4$]** (see Table 3). This trend could be rationalized by again considering the organization of the luminescent assemblies imparted by the inner nanotube diameter. In fact, inside large SWCNTs the resultant **1·[EuL$_4$]** assemblies were well-preserved and separated, which was not the case inside DWCNTs and MWCNTs. The more chaotic filling of their internal channel leads to the instauration of indiscriminate interactions between several C_{60} cages and a single Eu(III) complex, causing, as already demonstrated in a previous paper,[25] quenching of the emission. Regarding the more complex lifetime patterns observed for **1·[EuL$_4$]@CNTs**, other factors need to be taken into account besides the local ordering imparted by the templating nanotube structure. In fact, the possible presence of other emitting Eu species inside the CNTs' cavities cannot be excluded to explain the bi-exponential excited state lifetimes of the hybrids. Modification of the structure of [**EuL$_4$**]$^-$ might have in fact occurred during the encapsulation process causing either the loss of one or more ligands, yielding [**EuL$_3$**] or [**EuL$_2$**]$^+$ species or the formation of clusters (Fig. 2c).

In-vitro cellular uptake study using a confocal microscope

As a proof of principle to demonstrate the possibility of employing the reported hybrid material in biological imaging essays, we performed the internalization of **1·[EuL$_4$]@SWCNTs** into cancerous cells, and monitored uptake *via* confocal imaging. Specifically, HeLa cells were incubated with **1·[EuL$_4$]@SWCNTs** coated with PEG-5000. Figure 6 (see also Fig. S12, S.I.) displays the confocal fluorescence microscopy images of the treated cells, with the red color corresponding to the emission of the internalized **1·[EuL$_4$]@SWCNTs**, and the blue color to the emission of the employed nuclear stain (DAPI). These images clearly denote that the biological media in which it has been dispersed does not quench the luminescence of the hybrid, and the luminescence signal remains clearly detectable even upon internalization in the cell. The hybrid appears as small agglomerates dispersed in the cytoplasm surrounding the DAPI-stained nucleus, as previously reported for *Okazaki*'s coronene hybrid, possibly indicating a phagocytosis internalization mechanism in which the hybrid remains trapped in lysosomes.[14]

Conclusions

In conclusion, we have successfully driven the encapsulation of Eu(III) complexes in CNTs, by designing and synthesizing a C_{60}-appended ionic liquid nano-carrier. This approach allowed us not only to increase the filling ratio within thinner tubes, namely single and double-walled CNTs, but also to control the organization of the chromophores within the tubular framework. Photophysical investigations showed that the entrapment in different CNTs causes a different degree of emission quenching. The luminescent materials have been injected in cells, and their emission detected by confocal imaging. In the future, appropriate organic functionalization of the external carbon wall,

optimization of the filling procedure and the use of different emissive complexes could lead to a brand new class of novel visible-light-emitting CNT-based hybrids. Such hybrid structures could be envisaged for the creation of sensor based-diagnostics, as indicated by the preliminary *in-vitro* experiments.

Acknowledgments

DB, LDC and ANK would like to thank the European research council (ERC) for supporting this research. The Namur-Strasbourg collaboration has been supported by the Science Policy Office of the Belgian Federal Government (BELSPO-IAP 7/05 project). DB also acknowledges the FRS-FNRS (FRFC contracts n° 2.4.550.09), the "Loterie Nationale", the "TINTIN" ARC project (09/14-023), the MIUR through the FIRB "Futuro in Ricerca" ("SUPRACARBON", contract n° RBFR10DAK6) and the University of Namur (internal funding). MP and OP acknowledge the Polish Ministry of Science & Higher Education (grant N°:938/7. PR UE/2009/7). MEF acknowledges the sectorial operational program for human resources development 2007-2013, co-financed by the European Social Fund (POSDRU 107/1.5/S/76841). MN would like to thank Italian MIUR (FIRB RBAP11C58Y ''NanoSolar'') for funding. ANK and TC thank the Nottingham Nanotechnology and Nanoscience Centre (NNNC) for access to TEM facilities, and EPSRC for funding. KK acknowledges the Hungarian National Research Fund (OTKA grant no. 105691). The authors thank Dr. M. Utczás for expert technical help with the $scCO_2$ fillling, and Florent Pineux for technical support for the TGA analysis.

References

1 P. Singh, S. Campidelli, S. Giordani, D. Bonifazi, A. Bianco and M. Prato, *Chem. Soc. Rev*., 2009, **38**, 2214.

2 a) A. Hashimoto, K. Suenaga, A Gloter, K Urita, S. Iijima. *Nature*, 2004, **430**, 870; b) K. Suenaga, H. Wakabayashi, M. Koshino, Y. Sato, K. Urita, S. Iijima, *Nat. Nanotechnol.*, 2007, **2**, 358; c) K. Hirahara, K. Saitoh, J. Yamasaki, N. Tanaka, *Nano Lett.*, 2006, **6**, 1778.

3 C. N. R. Rao, B. C. Satishkumar, A. Govindaraj and M. Nath, *ChemPhysChem,* 2001, **2**, 78.

4 A. N. Khlobystov, *ACS Nano,* 2011, **5**, 9306.

5 D. A. Britz and A. N. Khlobystov, *Chem. Soc. Rev*., 2006, **35**, 637.

6 H. Ulbricht, G. Moos and T. Hertel, *Phys. Rev. Lett.,* 2003, **90**, 095501.

7 a) S. Berber, Y. K. Kwon and D. Tomanek, *Phys. Rev. Lett*., 2002, **88**, 185502; b) L. A. Grifalco and M. Hodak, *Phys. Rev. B,* 2002, **65**, 125404.

8 B. W. Smith, M. Monthioux and D. E. Luzzi, *Nature,* 1998, **396**, 323.

9 J. R. Lakowicz, "Principles of Fluorescence Spectroscopy", Springer (New York), 2006.

10 M. Shimizu and T. Hiyama, *Chem. Asian J*., 2010, **5**, 1516.

11 a) D. Parker and J. A. G. Williams, *J. Chem. Soc. Dalton Trans*., 1996, 3613; b) J. P. Leonard, C. B. Nolan, F. Stomeo and T. Gunnlaugsson, *Top. Curr. Chem*., 2007, **281**, 1.

12 K. Yanagi, Y. Miyata and H. Kataura, *Adv. Mater*., 2006, **18**, 437.

13 a) M. Yudasaka, K. Ajima, K. Suenaga, T. Ichihashi, A. Hashimoto, S. Iijima, *Chem. Phys. Lett*., 2003, **380**, 42; b) F. Simon, H. Kuzmany, H. Rauf, T. Pichler, J. Bernardi, H. Peterlik, L. Korecz, F. Fulop, A. Janossi, *Chem. Phys. Lett*., 2004, **383**, 362; c) M. Monthioux, *Carbon,* 2002, **40**, 1809; d) T. Takenobu, T. Takano, M. Shiraishi, Y. Murakami, M. Ata, H. Kataura, Y. Achiba, Y. Iwasa, *Nat. Mater*., 2003, **2**, 683; e) J. Gao, P. Blondeau, P. Salice, E. Menna, B. Bartova, C. Hebert, J. Leschner, U. Kaiser, M. Milko, C. Ambrosch-Draxl, M. A. Loi, *Small,* 2011, **13**, 1807; f) J. Mohanraj, N. Armaroli, *J. Phys. Chem. Lett.*, 2013, **4**, 767.

14 T. Okazaki, Y. Iizumi, S. Okubo, Dr. H. Kataura, Z. Liu, K. Suenaga, Y. Tahara, M. Yudasaka, S. Okada and S. Iijima, *Angew. Chem Int. Ed.,* 2011, **50**, 4853.

15 a) A. V. Talyzin, I. V. Anoshkin, A. V. Krasheninnikov, R. M. Nieminen, A. G. Nasibulin, H. Jiang, E. I. Kauppinen, *Nano Lett*., 2011, **11**, 4352; b) M. Fujihara, Y. Miyata, R. Kitaura, O. Nishimura, C. Camacho, S. Irle, Y. Iizumi, T. Okazaki, H. Shinohara, *J. Phys. Chem. C,* 2012, **116**, 15141; c) B. Botka, M. E. Füstös, G. Klupp, D. Kocsis, E. Székely, M. Utczás, B. Simándi, Á. Botos, R. Hackl, K. Kamarás, *Phys. Status Solidi B*, 2012, **249**, 2432; d) B. Botka, M. E. Füstös, H. M. Tóháti, K. Németh, G. Klupp, Zs. Szekrényes, D. Kocsis, M. Utczás, E. Székely, T. Váczi, G. Tarczay, R. Hackl, T. W. Chamberlain, A. N. Khlobystov, K. Kamarás, *Small,* 2013, DOI: 10.1002/smll.201302613.

16 a) K. Binnemans, "Handbook on the Physics and Chemistry of Rare Earths", Vol. **35**, Elsevier (Amsterdam), 2005; b) S. Quici, M. Cavazzini, G. Marzanni, G. Accorsi, N. Armaroli, B. Ventura, F. Barigelletti, *Inorg. Chem.*, 2005, **44**, 529; c) S. Quici, G. Marzanni, A. Forni, G. Accorsi, F. Barigelletti, *Inorg. Chem*., 2004, **43**, 1294; d) L. Armelao, G. Bottaro, S. Quici, M. Cavazzini, MC. Raffo, F. Barigelletti, G. Accorsi, *Chem. Commun*., 2007, 2911.

17 T. Pagnot, P. Audebert and G. Tribillon, *Chem. Phys. Lett*., 2000, **322**, 572.

18 a) K. Binnemans, *Chem. Rev*., 2009, **109**, 4283; b) J. C. G. Bunzli and S. V. Eliseeva, *J. Rare Earths,* 2010, **28**, 824.

19 a) L. D. Carlos, R. A. S. Ferreira, V. D. Bermudez and S. J. L. Ribeiro, *Adv. Mater*., 2009, **21**, 509; b) K. Binnemans and C. Görller-Wallrand, *Chem. Rev*., 2002, **102**, 2303; c) L. Maggini and D. Bonifazi, *Chem. Soc. Rev.,* 2012, **41**, 211.

20 a) G. Accorsi, N. Armaroli, A. Parisini, M. Meneghetti, R. Marega, M. Prato and D. Bonifazi, *Adv. Funct. Mater*., 2007, **17**, 2975.

21 H.-X. Wu, W.-M. Cao, J. Wang, H. Yang and S.-P. Yang, *Nanotechnology,* 2008, **19**, 345701.

22 a) L. Kong, J. Tang, J. Liu, Y. Wang, L. Wang and F. Cong, *Mater. Sci. Eng. C,* 2009, **29**, 85; b) C. Zhao, Y. Song, K. Qu, J. Ren and X. Qu, *Chem. Mater.,* 2010, **22**, 5718; c) X. Xin, M. Pietraszkiewicz, O. M. Pietraszkiewicz, O. Chernyayeva, T. Kalwarczyk, E. Gorecka, D. Pociecha, H. Li and R. Hoyst, *Carbon,* 2012, **50**, 436.

23 D. R. Kauffman, C. M. Shade, H. Uh, S. Petoud and A. Star, *Nat. Chem.,* 2009, **1**, 500.

24 B. Sitharaman, S. Rajamani and K. A. Pramod, *Chem. Commun*., 2011, **47**, 1607.

25 L. Maggini, H. Traboulsi, K. Yoosaf, J. Mohanraj, J. Wouters, O. Pietraszkiewicz, M. Pietraszkiewicz, N. Armaroli and D. Bonifazi, *Chem. Commun*., 2011, **47**, 1625.

26 L. Maggini, F. M. Toma, L. Feruglio, J. M. Malicka, T. Da Ros, N. Armaroli, M. Prato and D. Bonifazi, *Chem. Eur. J.,* 2012, **18**, 5889.

27 L. Maggini, M. Liu, Y. Ishida and D. Bonifazi, *Adv. Mater.*, 2013, **25**, 2462.

28 L. Maggini, J. Mohanraj, H. Traboulsi, A. Parisini, G. Accorsi, N. Armaroli and D. Bonifazi, *Chem. Eur. J*., 2011, **17**, 8533.

29 J. Fan, T. W. Chamberlain, Y. Wang, S. Yang, A. J. Blake, M. Schröder and A. N. Khlobystov, *Chem. Commun.,* 2011, **47***,* 5696.

30 S. Gago, J. A. Fernandes, J. P. Rainho, R. A. S. Ferreira, M. Pillinger, A. A. Valente, T. M. Santos, L. D. Carlos, P. J. A. Ribeiro-Claro and I. S. Goncalves, *Chem. Mater*., 2005, **17**, 5077.

31 K. Lunstroot, K. Driesen, P. Nockemann, C. Görller-Wallrand, K. Binnemans, S. Bellayer, J. Le Bideau and A. Vioux, *Chem. Mater.,* 2006, **18**, 5711.

32 S. M. Bruno, R. A. S. Ferreira, F. A. A. Paz, L. D. Carlos, M. Pillinger, P. Ribeiro-Claro and I. S. Gonçalves, *Inorg. Chem.,* 2009, **48**, 4882.

33 M. Poliakoff and P. J. King, *Nature,* 2001, **412**, 125.

34 A. N. Khlobystov, D. A. Britz, J. Wang, S. A. O'Neil, M. Poliakoff and G. A. D. Briggs, *J. Mater. Chem*., 2004, **14**, 2852.

35 N. Patel, R. Biswas and M. Maroncelli, *J. Phys. Chem. B,* 2002, **106**, 7096.

36 Á. Botos, A.N. Khlobystov, B. Botka, R. Hackl, E. Székely, B. Simándi, K. Kamarás, *Phys. Status Solidi B,* 2010, **247**, 2743.

37 a) For SWCNTs: D. Bonifazi, C. Nacci, R. Marega, G. Ceballos, S. Modesti, M. Meneghetti and M. Prato, *Nano Lett.,* 2006, **6**, 1408; b) for DWCNTs: R. Marega, G. Accorsi, M. Meneghetti, A. Parisini, M. Prato and D. Bonifazi, *Carbon,* 2009, **47**, 675; c) for MWCNTs: B. Kim, W. M. Sigmund, *Langmuir* 2004, **20**.

38 M. Zhang, M. Yudasaka, S. Bandow and S. Iijima, *Chem. Phys. Lett*., 2003, **369**, 680.

39 a) I. W. Chiang, B. E. Brinson, A. Y. Huang, P. A. Willis, M. J. Bronikowski, J. L. Margrave, R. E. Smalley and R. H. Hauge, *J. Phys. Chem. B*, 2001, **105**, 8297; b) J. Zhao, Y. Su, Z. Yang, L. Wei, Y. Wang and Y. Zhang, *Carbon*, 2013, **58**, 92.

40 T. W. Chamberlain, N. R. Champness, M. Schroder, and A. N. Khlobystov, *Chem. Eur. J.*, 2011, **17**, 668.

41 a) A. Dossing, *Eur. J. Inorg. Chem*., 2005, **8**, 1425; b) A. Beeby, I. M. Clarkson, R. S. Dickins, S. Faulkner, D. Parker, L. Royle, A. S. de Sousa, J. A. G. Williams and M. Woods, *J. Chem. Soc., Perkin Trans.*, 1999, **2**, 493.

42 J.-C. G. Bunzli, "Luminescent Probes", in Lanthanide Probes in Life, Chemical and Earth Sciences, Theory and Practice, ed. J.-C. G. Bunzli, G. R. Choppin, Elsevier, New York, 1989, p. 219.

43 J. H. Fosberg, *Coord. Chem. Rev*., 1973, **10**, 195.

Entry for the Table of Contents

C_{60}-driven efficient encapsulation of a luminescent Eu(III) complex inside carbon nanotubes

Laura Maggini, Melinda-Emese Füstös, Thomas W. Chamberlain, Cristina Cebrián, Mirco Natali, Marek Pietraszkiewicz, Oksana Pietraszkiewicz, Katalin Kamarás, Luisa De Cola, Andrei N. Khlobystov, and Davide Bonifazi

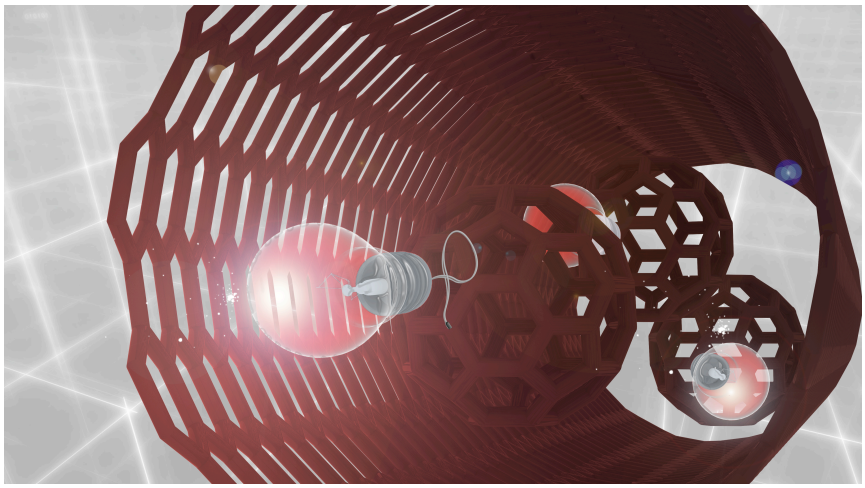

"Bullet of light". High-performance encapsulation of an Eu(III) complex inside carbon nanotubes was obtained when the encapsulated-to-be complex was designed possessing a C_{60}-fullerene moiety. Indeed, the fullerene's affinity for the inner channel of CNTs acts as the activating force for the ordered and oriented access of the Eu(III) complex inside CNTs, giving rise to an exciting novel luminescent hybrid material.

C_{60}-driven efficient encapsulation of a luminescent Eu(III) complex inside carbon nanotubes

Laura Maggini,[a,b] Melinda-Emese Füstös,[c,d] Thomas W. Chamberlain,[e] Cristina Cebrián,[b] Mirco Natali,[b,f] Marek Pietraszkiewicz,[g] Oksana Pietraszkiewicz,[g] Edit Székely,[h] Katalin Kamarás,[c] Luisa De Cola,[b] Andrei N. Khlobystov,[e] and Davide Bonifazi*[a,i]

[a] Namur Research College (NARC), University of Namur (UNamur), Rue de Bruxelles 61, 5000 Namur Belgium
E-mail: davide.bonifazi@unamur.be

[b] Institut de Science et d'Ingénierie Supramoléculaires (ISIS), Alleé Gaspard Monge 8, 67000 Strasbourg, France

[c] Institute for Solid State Physics and Optics, Wigner Research Centre for Physics, Hungarian Academy of Sciences, Konkoly-Thege M. 29-33, 1121 Budapest, Hungary

[d] Faculty of Chemistry and Chemical Engineering, Babeş-Bolyai Univeristy, Arany János 11, 400028 Cluj-Napoca, Romania

[e] School of Chemistry, University of Nottingham, University Park, Nottingham, NG7 2RD (UK)

[f] M. Natali, Department of Chemical and Pharmaceutical Sciences, University of Ferrara,Via Fossato di Mortara 17-19, 44121, Ferrara, Italy

[g] Institute of Physical Chemistry, Polish Academy of Sciences, PL-01224 Warsaw, Kasprzaka 44/52, Poland

[h] Department of Chemical and Environmental Process Engineering, Budapest University of Technology and Economics, Budafoki út 8, 1111 Budapest, Hungary

[i] Department of Chemistry and Pharmaceutical Sciences, INSTM UdR Trieste, University of Trieste (UNITS), Piazzale Europa 1, 34127 Trieste Italy

Supporting Information

Instruments and methods

Nuclear magnetic resonance spectroscopy (NMR). ^{1}H and ^{13}C spectra were obtained on a 400 MHz Jeol JNM EX-400 NMR. Chemical shifts were reported in ppm according to tetramethylsilane using the solvent residual signal as an internal reference (*d*-chlorophorm: $\delta_H = 7.26$ ppm, $\delta_C = 77.16$ ppm). Coupling constants (*J*) were given in Hz. Resonance multiplicity was described as *s* (singlet), *d* (doublet), *t* (triplet), *dd* (doublet of doublets), *dt* (doublet of triplets), *q* (quartet), *m* (multiplet) and *br* (broad signal). Carbon spectra were acquired with a complete decoupling for the proton.

Thermogravimetric analysis (TGA). All the TGAs were performed with a *TGA Q500* instrument manufactured by TA instruments (Italy), under N_2/air (80:20) flow of 55 ml·min^{-1} generally employing the following method: equilibration from room temperature to 50 °C, isothermal heating at 50 °C for 20 minutes, then thermal ramp from 50 °C to 800 °C with a heating rate of 2 °C·min^{-1}.
The loss of weight is extracted as a difference by the weight % and evaluated at the plateau of the curve for each derivative. μmol/mg are calculated using these two formula:

1000 mg : x = 100% : Loss of weight % (1)

$$\frac{mmol}{mg} = \left(x / MW\right) / mg \quad (2)$$

X-ray Photoelectron Spectroscopy (XPS). Studies were performed with a SSX-100 system (Surface Science instrument). The photon source was a mono-chromatized Al Kα line ($h\nu$ = 1486.6 eV) applied with a takeoff angle of 35°. In the spectrum analysis, the background signal was subtracted by Shirley's method. The C 1s core level peak position of carbon atoms was taken as the reference at 284.5 eV. The spectrum analysis was carried out by fitting the peak shape obtained in the same analyzing conditions and other components with mixed (Gaussian + Lorentzian) line shapes. XPS atomic ratios have been estimated from the experimentally determined area ratios of the relevant core lines, corrected for the corresponding theoretical atomic cross-sections and for a square root dependence of the photoelectron kinetics energies. At least three spots of 800 μm^2 per sample were characterized and the results are expressed as mean ± standard deviation.

Attenuated Total Reflectance Infrared Spectroscopy (ATR-IR).

Attenuated total reflectance (ATR) investigations in the infrared range (400-4000 cm^{-1}) were

performed on pristine and functionalized samples. For the measurements a Bruker Tensor 37 spectrometer was used with a Bruker Helios ATR-attachment employing a single-bounce germanium ATR crystal, with spectral resolution 1 cm^{-1}. Spectra were taken on the samples as received, no further sample manipulation was applied. All measured samples were in powder form. All measurements were completed in ambient conditions, each sample studied at 3-4 different spots (spot size 250 μm^2).

Supercritical CO_2 ($scCO_2$) induced peapod synthesis.

The high-pressure reactor used for the experiments was described in detail elsewhere [György Bánsághi, Edit Székely, David Méndez Sevillano, Zoltán Juvancz, Béla Simándi: Diastereomer salt formation of ibuprofen in supercritical carbon dioxide, J. of Supercritical Fluids 69 (2012), 113-116]. Freshly distilled carbon dioxide was carried by a pump through an inlet valve into the 36 ml stainless steel reactor vessel. The reactor is equipped with a pressure transducer, a thermocouple and a rupture disc. Adequate mixing was ensured by a stir bar rotated by a magnetic stirrer. The reactor was maintained at a constant temperature (50 °C) via thermostated water flowing through the reactor's aluminum jacket, circulated by a thermostat. The pressure was kept constant 15 MPa for 96 hours after starting the mixing. When the desired time elapsed, the reactor was cooled to 25 °C (pressure droped to 6.7 MPa). The reactor was depressurized slowly (approx. 40 min) by taking the gaseous phase of carbon dioxide. Carbon dioxide leaving the reactor passed through a filter and an outlet valve where it expanded to atmospheric pressure and was bubbled through methanol. The dry sample was collected from the reactor after depressurization.

High Resolution Transmission Electron Microscopy (HRTEM). Nanotube samples were dispersed in isopropanol and drop cast onto lacey carbon coated copper TEM grids for HRTEM analysis. HRTEM analysis was performed on a JEOL-2100F TEM microscope with a resolution limit of 0.2 nm. The imaging conditions were carefully tuned by lowering the accelerating voltage of the microscope to 100 kV and reducing the beam current density to a minimum in an attempt to minimise the electron beam induced damage of the sample. EDX spectra were recorded for small bundles of nanotubes (3-10 tubes) on a JEOL 2100F TEM equipped with an Oxford Instruments X-rays detector at 100 kV.

Photoluminescence measurements (PL). Steady-state emission and excitation spectra were recorded in front face mode on a HORIBA Jobin-Yvon IBH FL-322 Fluorolog 3 spectrometer equipped with a 450 W Xenon arc lamp and a TBX-4-X single-photon-counting as excitation source and detector, respectively. Emission spectra were corrected for source intensity (lamp and grating) and emission

spectral response (detector and grating) by standard correction curves. Photoluminescence decays were measured with a FluoTime 300 "EasyTau" apparatus (PicoQuant) equipped with subnanosecond LDH sources (375, 405, 440, 510 and 640 nm, 50-100 ps pulsewidth) powered by a PicoQuant PDL 820 variable (0.2-80 MHz) pulsed power supply. A PMA-C and a Hamamatsu H10330 PMT were employed for detection in the UV-visible (200-900 nm) and IR (900-1400 nm) respectively. Measurements were performed using a NanoHarp 250 MCS (Multichannel Scaler Card) histogram accumulating real-time processor. The decays were analyzed by means of PicoQuant FluoFit Global Fluorescence Decay Analysis Software. For solid-state measurements KBr discs were used, characterized by a sample concentration of 1 mg of carbonaceous derivative diluted in 3 mg of KBr. Photoluminescence quantum yields (PLQY) were calculated according to Equation 1, with τ_{obs} and τ_{rad} representing the measured and radiative lifetimes respectively [D. Parker, J. A. G. Williams, J. Chem. Soc. Dalton Trans. 1996, 3613; J.-C. G. Bünzli, Chem. Rev. 2010, 110, 2729; F. S. Richardson, Chem. Rev. 1982, 82, 541]:

$$\Phi_{Eu} = \frac{\tau_{obs}}{\tau_{rad}} \qquad (1)$$

$$\frac{1}{\tau_{rad}} = A_{MD,0} \times n^3 \times \left(\frac{I_{tot}}{I_{MD}} \right) \qquad (2)$$

τ_{rad} can in turn be estimated according to Equation 2 taking in account the amplitude weighted averaged lifetime values for τ_{obs}. $A_{MD,0}$ is the probability of the spontaneous $^5D_0 \rightarrow {}^7F_1$ decay (14.65 s^{-1}), n is the refractive index of the medium (air, 1.0008), I_{tot} is the area of the Eu (III) emission spectrum and I_{MD} is the area of the $^5D_0 \rightarrow {}^7F_1$ band.

***In-vitro* cell uptake experiments**. An aqueous suspension of polyethylene glycol (PEG-5000 MW) coated **1**·[**EuL$_4$**]**@SWCNTs** was prepared for *in-vitro* cellular uptake experiments. First **1**·[**EuL$_4$**]**@SWCNTs** were debundled and dispersed in a 10 % w/w water solution of PEG-5000 by sonication (3 hrs). The suspension was then ultra centrifuged at 25 krpm for 30 minutes to remove residual bundles, and the surnatant recovered for cellular uptake studies. HeLa cells cells were cultured in Dulbecco's modified Eagle medium (DMEM) supplemented with 10 % fetal bovine serum, 1% penicillin and streptomycin at 37 °C in 5 % CO_2/air atmosphere with 95 % relative humidity. The cells were placed in 35 mm glass-bottom culture dishes and grown overnight. Subsequently, 50 μl of the aqueous dispersion of **1**·[**EuL$_4$**]**@SWCNTs** were diluted with 2 ml of DMEM culture media and fed to the cells, previous to 24 hrs incubation. Following to the medium removal and washing with

phosphate-buffered saline protocols, the HeLa cells were fixed with paraformaldehyde and finally stained with 4,6-diamidino-2-phenylindole dihydrochloride (DAPI) for 1 min.

Confocal imaging. Cell samples were imaged using a Zeiss LSM-710 microscope (Carl Zeiss), using an excitation laser at 405 nm.

Materials and reagents. Chemicals and solvents were purchase from Sigma Aldrich and used without further purification. Deuterated solvents were purchased from Eurisotop. SWCNTs were purchased from Carbon Solutions (P2-SWNT). DWCNTs and MWCNTs were kindly provided by Nanocyl. HeLa cells were obtained from ATCC/LGC Standards GmbH (Wesel, Germany). 4,6-diamidino-2-phenylindole dihydrochloride (DAPI, nuclear stain) was purchased from Polysciences Europe GmbH (Eppelheim, Germany).

Synthesis

1-(5-Hydroxypentyl)-3-ethylimidazolium bromide (2)

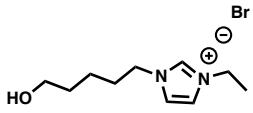

N-ethylimidazole (960 mg, 10 mmols) was refluxed with 5-bromopentanol (1.84g, 11 mmols) in 50 ml of toluene for 16 hours. After cooling to r.t., evaporation of the solvent under reduced pressure, afforded the product **2** (95%) as a colorless oil. ^{1}H-NMR (d_6-DMSO): δ 9.27 (*s*, 1H; -NC*H*N), 7.83 (*m*, 2H; -NC*HCH*N), 4.19 (*m*, 4H; the two -NCH_2), 3.37 (*t*, 2H; -CH_2OH), 1.80 (*m*, 2H; -(CH$_2$)$_3$CH$_2$CH_2OH), 1.43 (*m*, 5H; -CH$_2$CH_3 and –CH$_2$CH_2(CH$_2$)$_3$OH), 1.27 (m, 2H; -(CH$_2$)$_2$CH_2(CH$_2$)$_2$OH); ^{13}C-NMR (d_6-DMSO): δ 135.65, 122.39, 122.12, 60.25, 48.83, 44.19, 31.64, 29.19, 22.14, 15.03. IR (cm^{-1}): ν 3374.02, 3136.85, 3078.54, 2934.68, 2865.47, 2069.98, 1567.65, 1452.56, 1164.07, 1048.98, 835.92, 755.05, 633.74. MS (LC-MS, ESI): found 183.12 [M]$^{+}$, $C_{10}H_{19}ON_2$ requires = 183.14.

1-(5-Bromopentyl)-3-ethylimidazolium bromide (3)

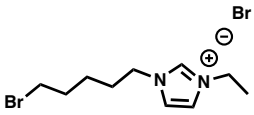

In order to obtain the active complex [Ph$_3$P-CBr$_3$]·Br, PPh$_3$ (3.14 g, 12 mmols) is first heated at 60° C with CBr$_4$ in CHCl$_3$ (50 ml) for 1 h. **2** (1.83 g, 10 mmols) was hence added and the reaction kept stirring for 12 hours at the reflux temperature. After allowing the reaction to reach r.t., evaporation of the solvent *in vacuo* afforded a residue which was dispersed in a small amount of MeOH (5 ml). Distilled water was then added (50 ml) with vigorous stirring. Filtration and subsequent concentration of the solution under reduced pressure yielded **3** (72%) as a brownish solid. M.p. 100-105 ºC; ^{1}H-NMR (d_6-DMSO): δ 9.40 (*s*, 1H; -NC*H*N), 7.86 (*m*, 2H; -NC*HCH*N), 4.19 (*m*, 4H; the two -NCH_2), 3.30 (*m*, 2H; -(CH$_2$)$_4$CH_2Br), 1.84 (*m*, 2H; -(CH$_2$)$_3$CH_2CH$_2$Br), 1.42 (*m*, 5H; -CH$_2$CH_3 and -(CH$_2$CH_2(CH$_2$)$_3$Br), 1.22 (*m*, 2H; -(CH$_2$)$_2$CH_2(CH$_2$)$_2$Br); ^{13}C-NMR (d_6-DMSO): δ 135.77, 122.40, 122.12, 48.40, 44.22, 28.58, 22.02, 15.05 (some signals are missing probably due to overlap). IR

(cm^{-1}): *v* 3416.72, 3087.56, 2059.75, 1631.61, 1563.43, 1454.20, 1166.82, 848.66, 754.82, 644.85. MS (LC-MS, ESI): found 245.08 $[M]^+$, $C_{10}H_{18}BrN_2$ requires = 245.06.

1-(5-Azidopentyl)-3-ethylimidazolium bromide (4)

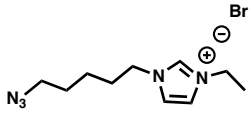

NaN_3 (195 mg, 3 mmols) was added to a solution of **3** (735 mg, 3 mmols) in MeOH (40 ml), and the resulting mixture stirred at reflux temperature for 24 hours. After cooling to r.t., the reaction was filtrated and the solution concentrated under vacuum. The crude was finally purified by hot filtration in CH_2Cl_2, affording compound **4** (80%) as a sticky yellow solid. M.p. 62-65 ºC; ^{1}H-NMR (d_6-DMSO): δ 9.36 (*s*, 1H; -NC*H*N), 7.84 (*m*, 2H; -NC*HCH*N), 4.20 (*m*, 4H; the two -NCH_2), 3.32 (*m*, 4H; -CH_2CH_2N$_3$), 1.84 (*m*, 2H; -CH$_2$CH_2(CH$_2$)$_3$N$_3$), 1.56 (*m*, 1H; -(CH$_2$)$_2$CH_2(CH$_2$)$_2$N$_3$ one of the two hydrogens of the group), 1.45 (*t*, 3H; -CH$_2$CH_3), 1.23 (*m*, 1H; -(CH$_2$)$_2$CH_2(CH$_2$)$_2$N$_3$); ^{13}C-NMR (d_6-DMSO): δ 135.76, 122.40, 122.12, 50.30, 48.39, 44.21, 28.57, 27.4, 22.68, 22.02, 15.05. IR (cm^{-1}): *v* 3532.68, 2105.49, 1562.05, 1447.71, 1162.46, 757.46, 636.92. MS (LC-MS, ESI): found 208.10 $[M]^+$, $C_{10}H_{18}N_5$ requires = 208.15.

N-5-(3-ethylimidazolium)-pentyl-bromide aza-[60] fullerene (1·Br)

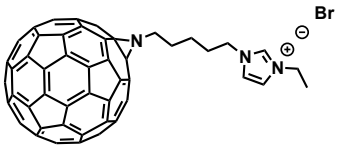

To a solution of C_{60} (504 mg, 0.7 mmols) in mesitylene/DMSO (1 : 1), a solution of **4** (146 mg, 0.7 mmols) in DMSO (5 ml) was added and the whole stirred at 140° C for 14 hrs. The precipitate formed during the reaction was filtered off and washed with H_2O. Precipitation upon addition of DMF, to a solution of the precipitate in CS_2 afforded **1·Br** (35%) as a golden solid insoluble in all common organic solvents. M.p. > 150 °C; IR (cm^{-1}): *v* 3436.1, 2918, 1618, 1429, 1182, 994, 527. MS (LC-MS, APCI): found 900.20 $[M]^+$, $C_{70}H_{18}N_3$ requires = 900.15.

N-5-(3-ethylimidazolium)-pentyl-[Eu(III)tetrakis(2-naphthoyltrifluoro-acetonato)] aza-[60] fullerene (1·[EuL$_4$])

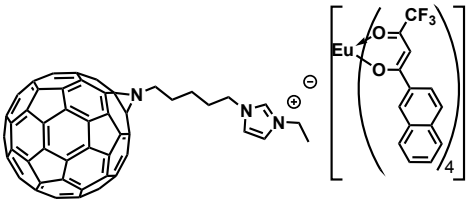

To a dispersion of the C_{60}-based carrier (**1·Br**; 10 mg, 0.01 mmols) in toluene an excess of the precursor ionic complex **NEt$_4$·[EuL$_4$]** (10-fold excess; 100 mg, 0.07 mmols) was added, and the mixture allowed to stir in air atmosphere and at r.t., for 14 hours. Precipitation in $CHCl_3$, followed by filtration on a Millipore apparatus and copious rinsing with $CHCl_3$ afforded the desired supramolecular complex as a brown powder (20 mg, 95 %). M.p. > 150 °C; IR (cm^{-1}): *v* 3436.1, 2918, 1618, 1500, 1429, 1250, 1182, 1150, 994, 750, 580, 527. MS (MALDI-MS): found 2113.30 $[M]^+$, $C_{134}H_{50}N_4EuF_{12}O_8$ requires = 2113.15.

Encapsulation of 1·[EuL$_4$]@CNTs

The encapsulation reaction of **1·[EuL$_4$]** in SWCNTs, DWCNTs and MWCNTs was performed in a high-pressure closed reactor employing supercritical carbon dioxide ($scCO_2$) as solvent. Before starting the reaction, CNTs were oxidized according to the required procedure, and subsequently annealed in air at 570 °C for 20 minutes to remove carboxylic groups at the entrance of the tube which might hamper the efficient encapsulation of the nano-carrier. Approximately 15 mg of **1·[EuL$_4$]** was inserted together with the oxidized CNTs (20 mg) in the reactor, which was subsequently sealed and filled with CO_2 at 150 bar (volume of solvent = 30 ml). The reaction was then heated at 50 °C and stirred for 96 hours. At the end of the reaction time the reactor was cooled to 25 °C and the resulting gaseous CO_2 bubbled in 8 ml of methanol until complete depressurization of the reactor. The product, **1·[EuL$_4$]@CNTs**, was finally collected and washed with CH_2Cl_2 to remove **1·[EuL$_4$]** adsorbed on the external walls of CNTs. Washings were monitored by UV-Vis absorption and IR-ATR (see Fig. S1).

Experimental Part

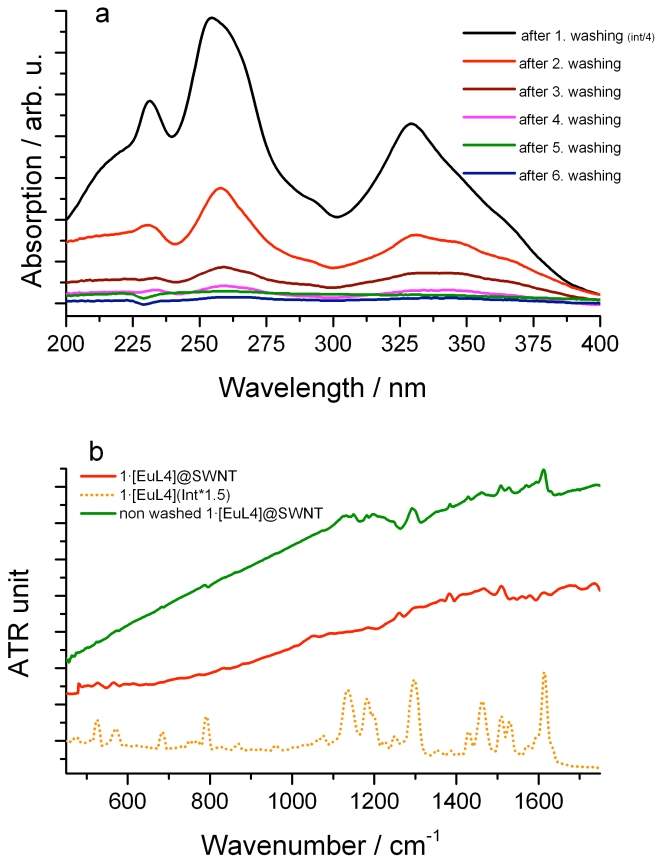

Figure S1. a) UV/VIS spectra of the washings performed on **1•[EuL$_4$]@SWCNTs**. After the sixth purification treatment, the concentration of **1•[EuL$_4$]** decreased below 0.001 mg/ml; b) ATR-IR spectra of **1•[EuL$_4$]** and **1•[EuL$_4$]@SWCNTs** before washing and after the sixth washing steps. Vibrational features of **1•[EuL$_4$]** disappear on washing, indicating that there is no significant amount of adsorbed species on the surface of the nanotubes.

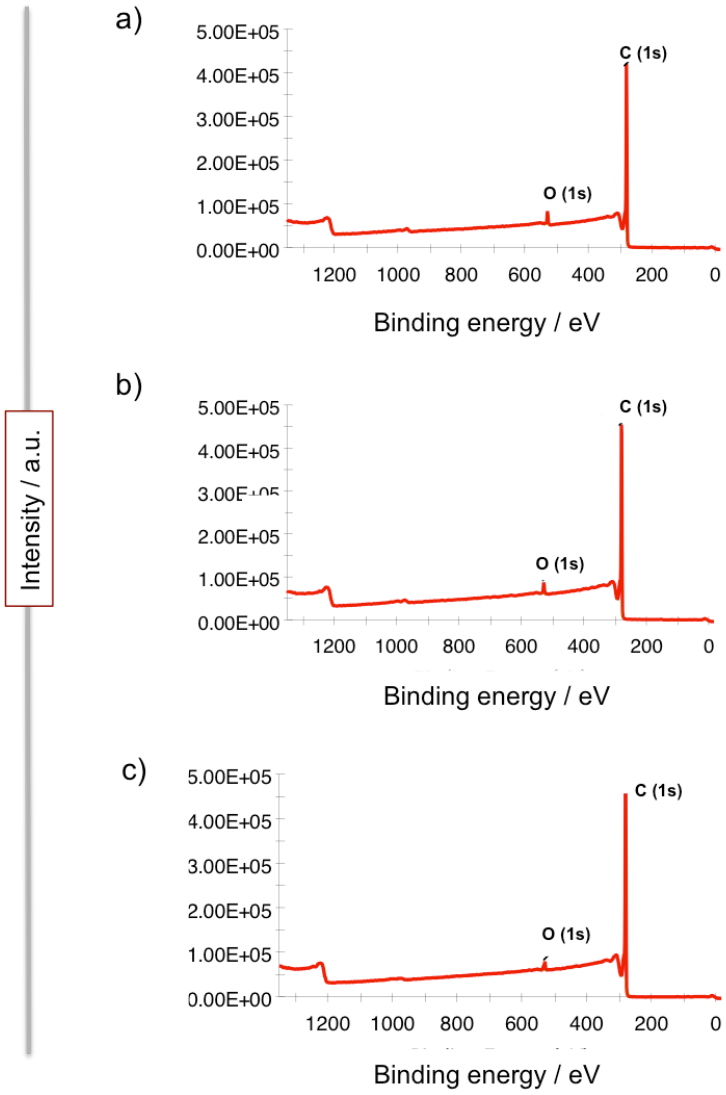

Figure S2. XPS survey spectra of: a) **ox-SWCNTs**, b) **ox-DWCNTs**, c) **ox-SWCNTs**. In the X axis the value represents the binding energy, expressed in eV, whilst for the Y axis arbitrary units represent the intensity of the signal.

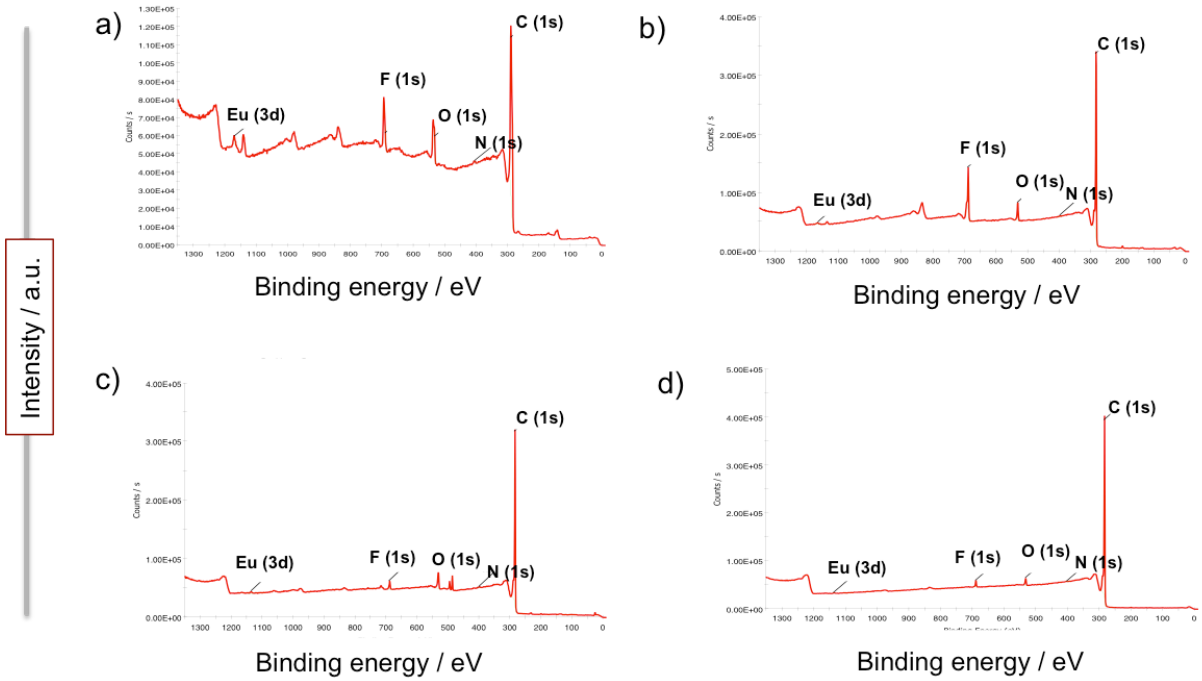

Figure S3. XPS survey spectra of: a) **1•[EuL$_4$]**, b) **1•[EuL$_4$]@SWCNTs**, c) **1•[EuL$_4$]@DWCNTs**, and d) **1•[EuL$_4$]@MWCNTs**. In the X axis the value represents the binding energy, expressed in eV, whilst for the Y axis arbitrary units represent the intensity of the signal.

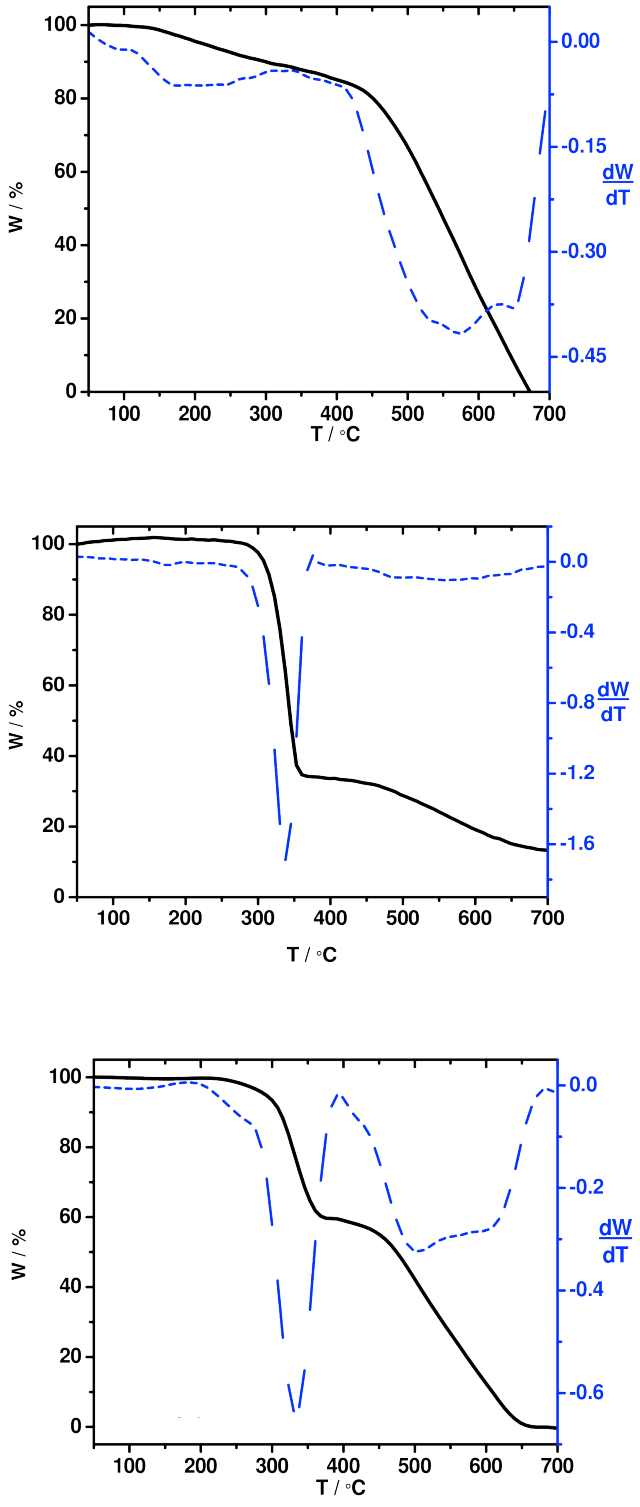

Figure S4. Thermogravimetric analysis for (from top to bottom): **4**; **1•Br**; **1•[EuL$_4$]**. The traces reported were recorded in N_2/air (80:20) atmosphere with a heating ramp of 2° C / min.

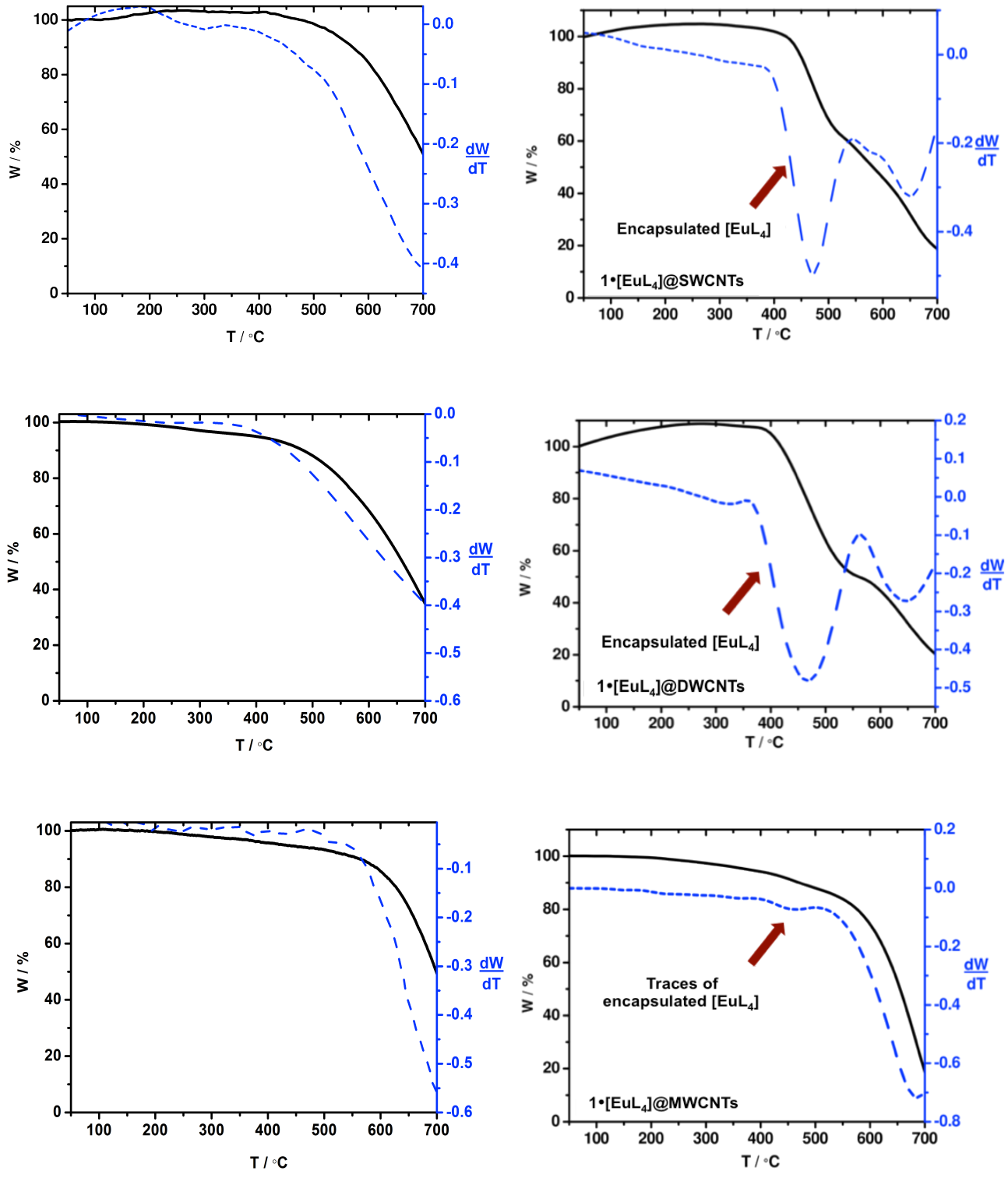

Figure S5. Thermogravimetric analysis for (from top to bottom): SW, DW and MWCNTs in their oxidized form (spectrum on the right) and corresponding encapsulation hybrid (spectrum on the left). The traces reported were recorded in N_2/air (80:20) atmosphere with a heating ramp of 2° C / min.

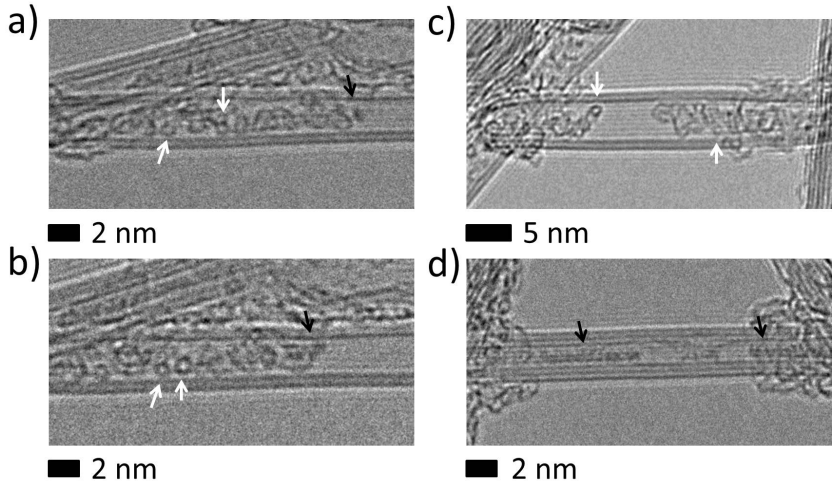

Figure S6. HRTEM images taken at 100 kV of a-d) **1•[EuL$_4$]@DWCNTs** in which fullerene cages (white arrows) and Eu metal clusters and rods (black arrows) are observed indicating successful introduction of the Eu complex into the internal channel of the DWCNTs.

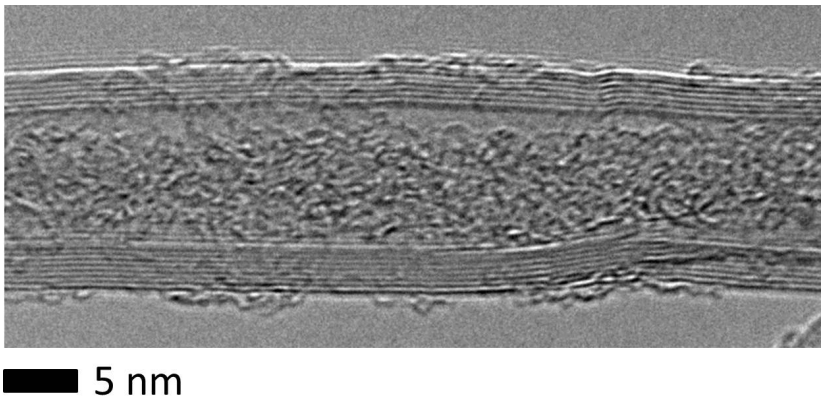

Figure S7. HRTEM image taken at 100 kV of **1•[EuL$_4$]@MWCNTs** showing significant filling of the internal channel.

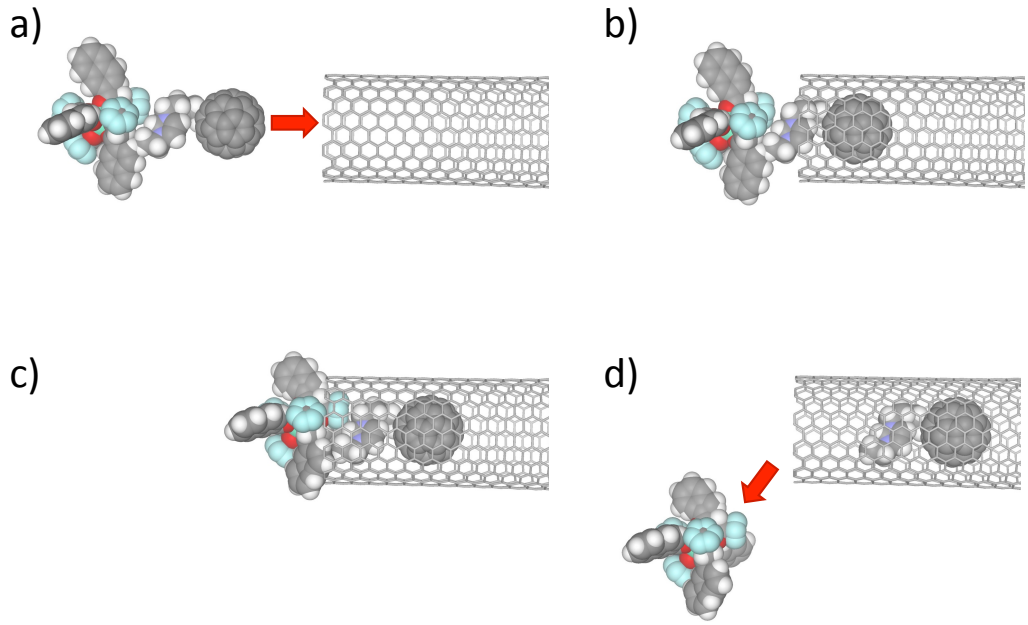

Figure S8. Schematic representation of the sequential encapsulation and the subsequent decomposition of **1•[EuL$_4$]** when entering SWCNTs, showing how the Eu containing complex is forced to dissociate from the fullerene part (d) as the fullerene moves progressively further into the SWCNT during encapsulation (d_{NT} = 1.4–1.5 nm).

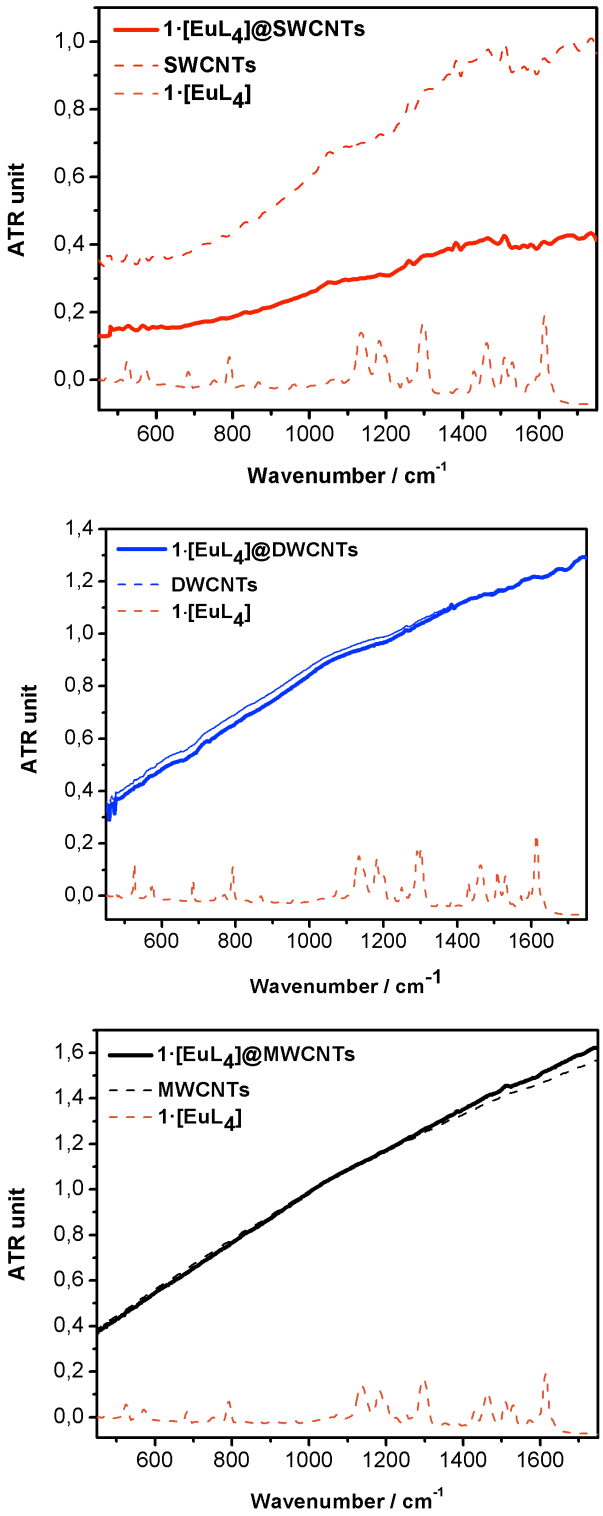

Figure S9. IR-ATR spectra of (from top to bottom): **1•[EuL$_4$]@SWCNTs**, **1•[EuL$_4$]@DWCNTs**, and **1•[EuL$_4$]@MWCNTs**. The lack of the intense signals of the Eu(III) complex indicates the absence of exohedral **1•[EuL$_4$]** confirming the efficiency of the cleaning procedure.

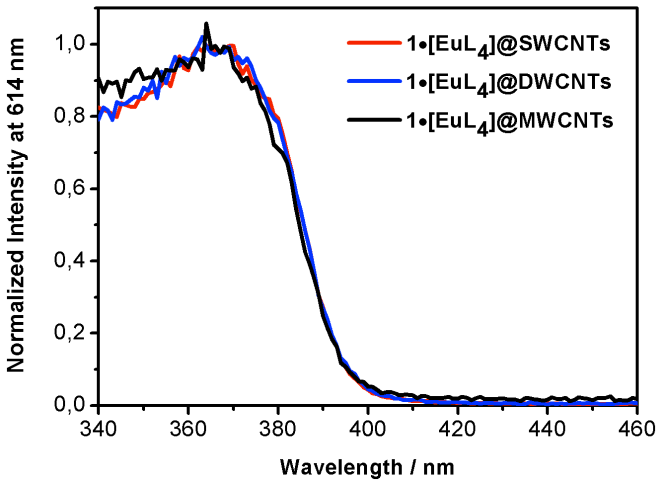

Figure S10. Excitation spectra of the Eu(III)-centred emission (recorded at 614 nm) of the three **1•[EuL$_4$]@CNTs** hybrids.

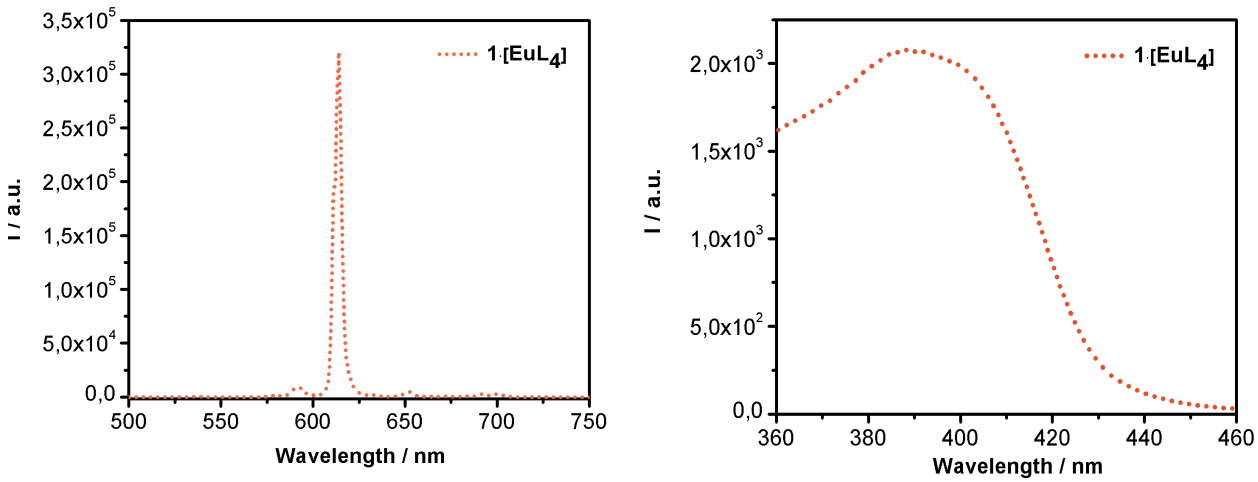

Figure S11. Emission (left, λ_{exc} = 475 nm) and excitation (right, recorded λ = 614 nm) spectra of **1•[EuL$_4$]**, performed in the solid state.

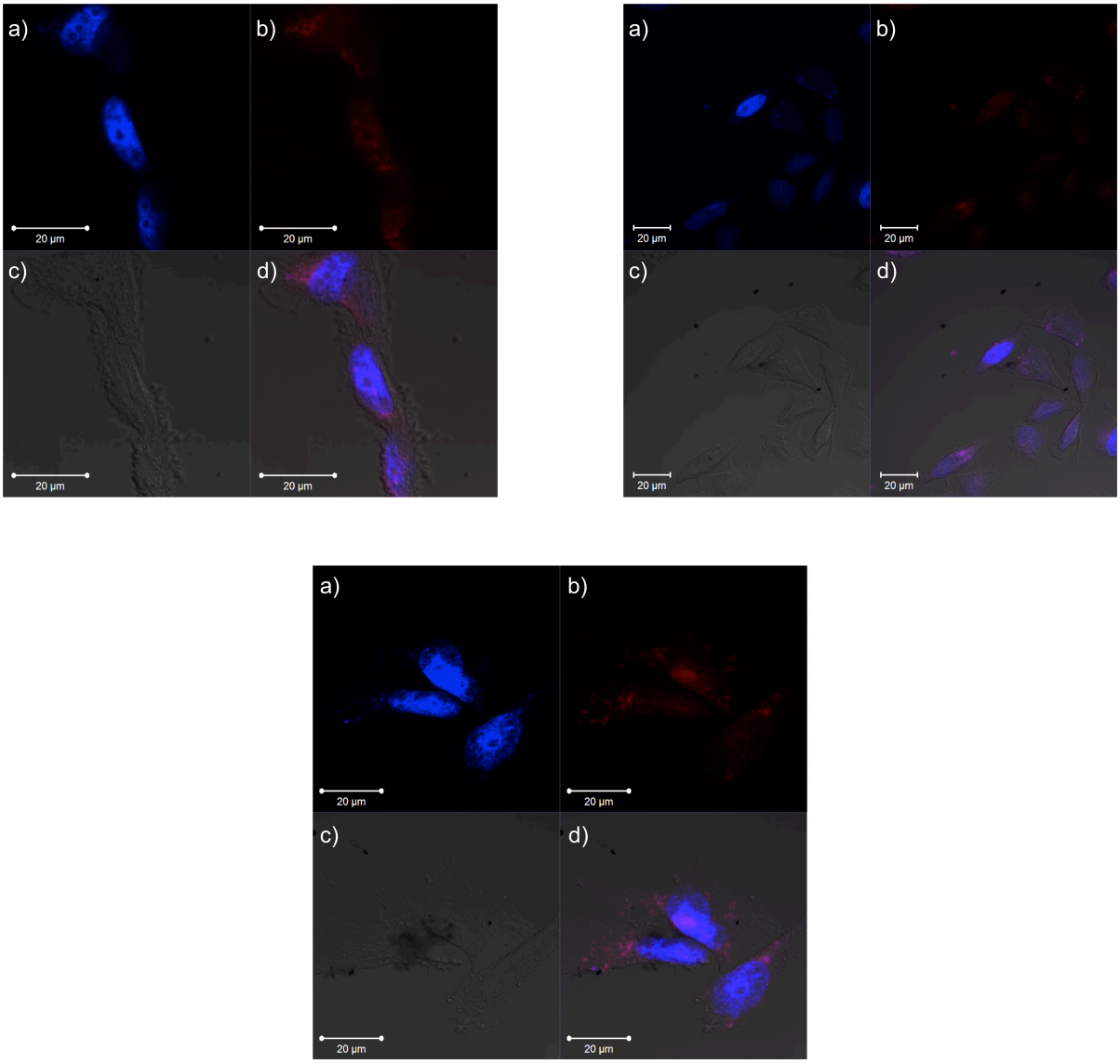

Figure S12. Confocal images of HeLa cells incubated for 24 hrs with **1•[EuL$_4$]@SWCNTs** wrapped in PEG-5000 polymer. a-c) separated detected channels: DAPI channel (a), Eu(III) channel (b) and PMT (c). d) overlapped image of the three channels.